



Article

Low-Cost Shadow Mask Fabrication for Nanoelectronics

Thomas Pucher ^{1,*}, Pablo Bastante ², Estrella Sánchez Viso ¹ and Andres Castellanos-Gomez ^{1,*}

¹ Materials Science Factory, Instituto de Ciencia de Materiales de Madrid (ICMM-CSIC), E-28049 Madrid, Spain; estrella.sanchez.viso@csic.es

² Departamento de Física de la Materia Condensada, Universidad Autónoma de Madrid, E-28049 Madrid, Spain; pablo.bastante@uam.es

* Correspondence: thomas.pucher@csic.es (T.P.); andres.castellanos@csic.es (A.C.-G.)

Abstract: We present two approaches for fabricating shadow masks for the evaporation of electrodes onto nanomaterials. In the first one, we combine the use of a commercial fiber laser engraving system with readily available aluminum foil. This method is suitable for fabricating shadow masks with line widths of 50 μm and minimum feature separation of 20 μm , and using it to create masks with complex patterns is very straightforward. In the second approach, we use a commercially available vinyl cutting machine to pattern a vinyl stencil mask, and we use a glass fiber to define the separation between the electrodes. With this approach, we achieve well-defined electrodes separated by 15 μm , but this technique is less versatile in creating complex masks as compared with the laser-based one. We demonstrate the potential of these techniques by fabricating field-effect transistor devices based on MoS_2 . Our approach is a cost-effective and easily accessible method for fabricating shadow masks with high resolution and accuracy, making it accessible to a wider range of laboratories.

Keywords: shadow mask deposition; rapid prototyping; micro-fabrication; device fabrication; field-effect transistor; two-dimensional materials



Citation: Pucher, T.; Bastante, P.; Sánchez Viso, E.; Castellanos-Gomez, A. Low-Cost Shadow Mask Fabrication for Nanoelectronics. *Nanomanufacturing* **2023**, *3*, 347–355. <https://doi.org/10.3390/nanomanufacturing3030022>

Academic Editor: Asterios (Stergios) Pispas

Received: 3 July 2023

Revised: 2 August 2023

Accepted: 8 August 2023

Published: 16 August 2023



Copyright: © 2023 by the authors. Licensee MDPI, Basel, Switzerland. This article is an open access article distributed under the terms and conditions of the Creative Commons Attribution (CC BY) license (<https://creativecommons.org/licenses/by/4.0/>).

1. Introduction

Electrode deposition is a critical step in the fabrication of electronic devices with nanomaterials. The most widely extended method to deposit electrodes is probably based on lithographic techniques, i.e., photolithography or electron beam lithography, which require specialized and expensive facilities as well as a strong technical background in micro-fabrication. Recent works show different approaches for lower-cost lithography setups used with nanomaterials [1,2]. Nevertheless, these lithographic techniques require chemical treatment steps to ensure the adhesion of the resists for the development and lift-off steps, which can harm certain nanomaterials that are more sensitive to the environment.

Direct metal evaporation through a shadow mask, on the other hand, has several advantages over conventional lithographic techniques [3–6]. For example, it is relatively inexpensive, easy to implement, and does not require a clean room environment. Additionally, it can be easily applied in labs that do not have a background or infrastructure in microfabrication. Another important aspect of the method is the fact that it is an ‘all-dry’ process, which means that it is also compatible with nanomaterials that tend to degrade or damage during the chemical and optical treatments involved in lithographic techniques [7–9]. Pre-patterned electrodes have the advantage of enabling a nanomaterial assembly in the glove box, which is crucial for air-sensitive materials [10,11].

Typically, shadow mask fabrication requires a specialized facility similar to those used for lithographic processing, which can be very costly [12,13]. Most research groups using shadow mask deposition buy commercially available masks or outsource the fabrication to micro-fabrication foundries, making the use of shadow mask deposition less flexible and unsuitable for rapid prototyping. This raises the question of whether there is a technique to fabricate shadow masks in a way that is affordable and flexible, which would allow

research groups to design and fabricate their own customized masks without the need for costly infrastructure or fabrication outsourcing.

Tomczyk et al. recently published a work about laser ablation fabrication of masks using homebuilt optical systems. However, these systems were typically composed of expensive components, and the resolution achieved was only in the 50 to 100 μm range [14]. This may not be sufficient for many applications with nanomaterials, which require electrodes in the 10–50 μm range. Moreover, the reported laser ablation setups are difficult to use and expensive to implement, making it not suitable for many research groups. Elhami Nik et al. also reported a recent work about the use of a CO_2 laser to ablate filter paper to create shadow masks, resulting in masks with a minimum feature size of 100 μm [15].

In this work, we present two approaches for fabricating shadow masks for the evaporation of electrodes to fabricate devices with nanomaterials, bridging the gap between flexibility in realizing the design and the cost factor. In the first method, we make use of a commercially available fiber laser engraving system (Atomstack M4, costing less than EUR 1100) with readily available metal supports (standard kitchen aluminum foil and thick aluminum foil) for shadow mask engraving of self-drafted layouts with maximum flexibility. In the second method, we use a vinyl cutting machine (Cricut Maker 3, under EUR 500) to create a vinyl stencil mask defining the electrodes and pads with pre-defined gap sizes and maximum cost-effectiveness. As the resolution of the vinyl cutter does not allow us to achieve electrode separation under 100 μm , we place a glass fiber (15 μm in diameter) to define the separation between the electrodes. We illustrate the potential of these methods by fabricating single-layer MoS_2 field-effect transistors.

2. Materials and Methods

Figure 1a shows a picture of the compact fiber laser engraving system used in this work while it cuts through aluminum foil. The system uses a pulsed IR laser (1064 nm) focused on a spot of ~ 20 μm and features two scanning galvanometer mirrors that allow it to reach a marking speed of up to 12 m/s. We found that standard kitchen aluminum foil can be used to fabricate well-defined shadow masks, but handling them without creating folds/wrinkles can be challenging (note that an example of a kitchen aluminum foil mask is given in the Supporting Information Figure S1). We thus tested thicker aluminum foil (40 μm thick, 150 \times 150 mm sheets, typically commercialized for use in shisha/hookah, LINK) that leads to optimal performance in terms of easiness to pattern and handle afterward. Figure 1b shows a picture of one of these thick aluminum foils, laser-cut to form a shadow mask with pads and drain-source electrodes separated by different gap sides, adhered to a SiO_2/Si substrate with Kapton tape prior to metal evaporation. The inset in the figure shows a higher magnification image of one of the 20 μm gaps. We found that masks designed with a drain-source separation under 20 μm tend to fail, thus leading to a shorted drain-source connection.

Figure 1c shows a picture of the other system tested to fabricate inexpensive homemade shadow masks: a vinyl cutter. The system operates very similarly to an old-fashioned XY plotter system, but uses a sharp blade tool instead of a pen. This kind of system, although inexpensive and very easy to use, cannot be used to make small features or structures with small pitch (that is, below a 200 μm feature or pitch size, the vinyl-cut masks are not reliable). To fabricate shadow masks with a smaller separation between drain and source electrodes, we combined the vinyl-cut mask with a glass fiber that is 15 μm in diameter to define the separation between drain and source electrodes without being limited by the vinyl-cutting system. Previous works using glass or carbon fibers as shadow masks have been reported in the literature to provide good-quality electrodes [16,17]. The combination with a vinyl cut mask can provide a more controlled way to deposit the metal electrodes and to pattern the pads and the leads to avoid shorts with other parts of the device or with the back gate. Figure 1d shows an optical image of one of the vinyl cut masks where one can appreciate the pads and the electrode leads. One can also notice the glass fiber deposited in the central part of the substrate before adhering to the vinyl cut mask to define

the drain-source separation. The inset shows a higher magnification image of the glass fiber, creating the separation between the electrodes.

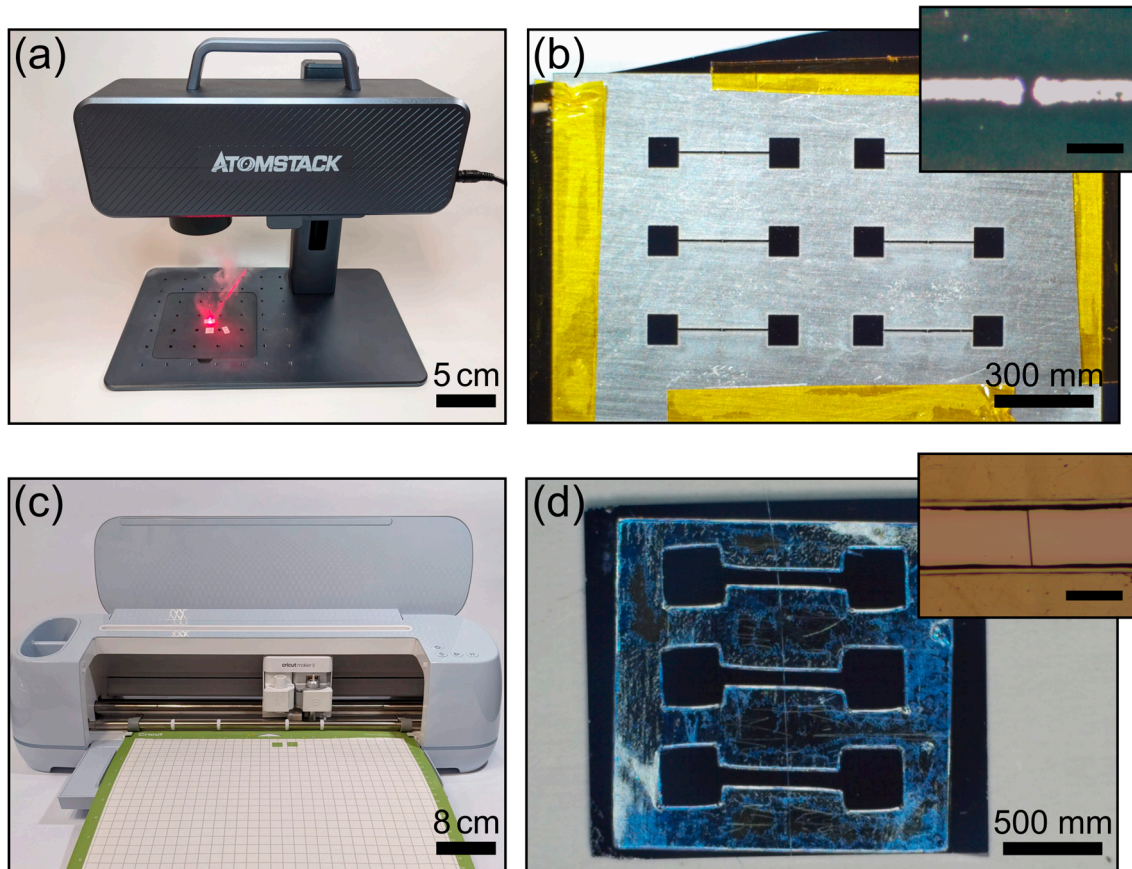


Figure 1. Fabrication of shadow masks with commercially available laser engraver and vinyl cutter systems. (a) Picture of a fiber laser engraving system Atomstack M4 while cutting thick aluminum foil. (b) Picture of one of the fabricated shadow masks with drain and source electrodes separated by different distances ranging from 20 μm to 40 μm , fixed on a SiO_2/Si substrate with Kapton tape. (Inset) Optical microscopy image of the separation between the drain and source electrode at the central part of the ‘bar-shaped’ lead. The scale bar is 100 μm . (c) Picture of a Cricut Maker 3 vinyl cutter system used to prepare a vinyl stencil mask with the pads and the electrode leads. (d) Vinyl mask adhered onto a SiO_2/Si substrate using the adhesive of the vinyl. A 15 μm diameter glass fiber was deposited onto the surface prior to adhering the mask to define the separation between drain and source electrodes (see inset, scale bar: 500 μm).

3. Results

3.1. Fabrication of Electrodes by Metal Deposition through the Masks

In the following, we characterize the electrodes achieved after metal deposition through the shadow masks. We employ an electron beam evaporation system to deposit 5 nm of Ti (adhesion layer) and 45 nm of Au. Figure 2a shows an optical image of a shadow mask fabricated onto the 40 μm thick aluminum foil by laser ablation. Figure 2b shows an optical image of a SiO_2/Si substrate after metal deposition that closely follows the shape of the shadow mask shown in Figure 2a. The inset in Figure 2b shows a higher magnification optical microscopy image of the gap between the drain and source electrodes. Figure 2c shows an optical image of a mask made with the combination of a glass fiber and a vinyl cut stencil. The mask is adhered onto a SiO_2/Si substrate before metal deposition. Figure 2d is an optical image of the SiO_2/Si substrate after metal deposition. The inset in 2d depicts a detail of the gap created between the drain and source with the glass fiber.

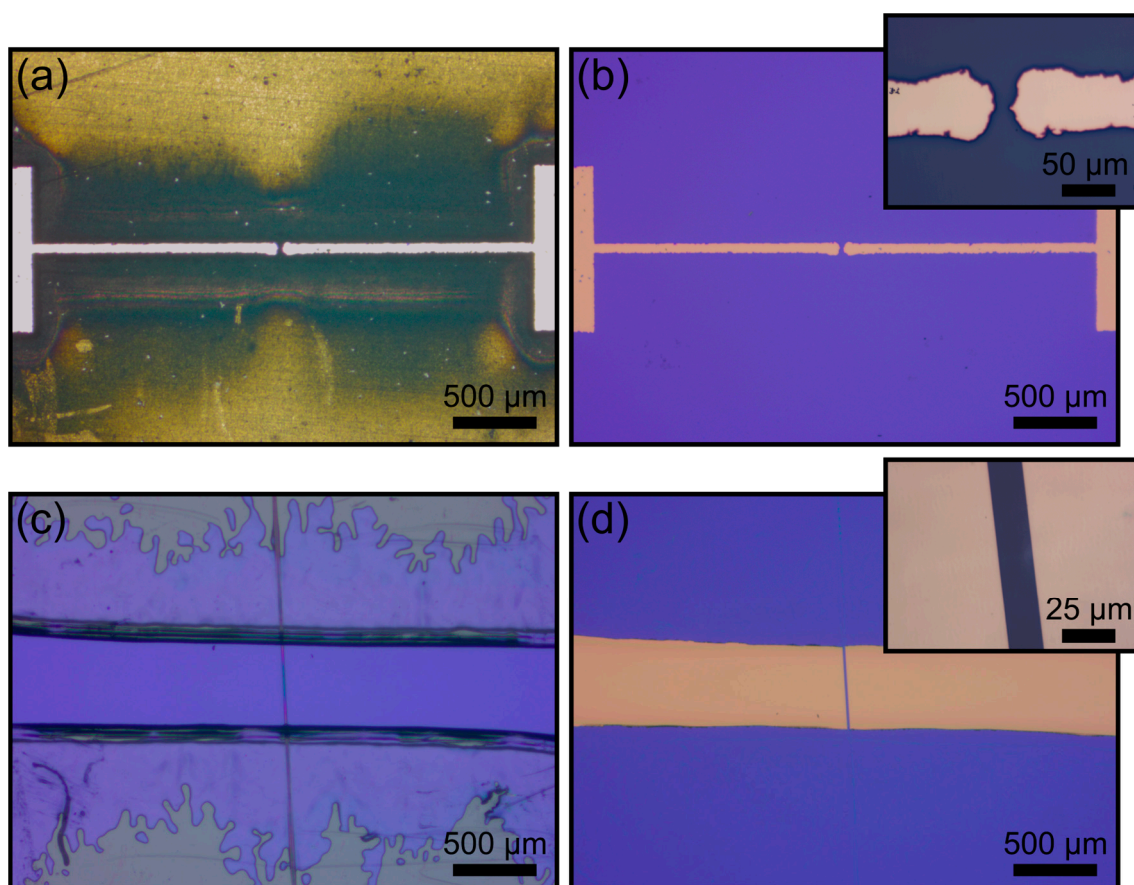


Figure 2. Resulting electrodes after evaporation through the homebuilt shadow masks. (a) Optical microscopy image of a drain-source mask patterned on thick aluminum foil with the fiber laser engraver system. (b) Optical microscopy image of the resulting electrodes after evaporating Au (45 nm)/Ti (5 nm) onto a SiO₂/Si substrate. (Inset) Higher magnification image of the gap between drain and source electrodes. (c) Optical microscopy image of a drain-source mask fabricated by combining the vinyl mask with a 15 μm diameter glass fiber adhered onto a SiO₂/Si before metal deposition. (d) Optical microscopy image of the resulting electrodes after evaporating Au (45 nm)/Ti (5 nm) onto a SiO₂/Si substrate. (Inset) Higher magnification image of the gap between drain and source electrodes.

As one can clearly see from Figure 2, we found that the vinyl + glass fiber approach yields very well-defined drain-source electrodes whose separation is directly defined by the diameter of the fiber. But, this technique suffers from lower flexibility in exploring different customized electrode designs. The laser engraving method, on the other hand, yields poorly defined electrode edges but ensures complete flexibility over the pattern design. This increased flexibility allows for the design and implementation of new patterns and layouts, providing more freedom in the design process and enabling more advanced electronic devices to be fabricated with nanomaterials. Additionally, this method can be used to quickly test different designs, which will allow for faster development and optimization of the fabrication process. In this way, the use of a commercially available fiber laser engraving system can open the door to additional flexibility in shadow mask fabrication, providing a powerful tool for researchers working in the field of nanoelectronics, whereas the use of a vinyl cutter in combination with glass fibers can provide the most cost-effective route to fabricate devices for research groups running under a moderate budget. We direct the reader to Figure S2 in the Supporting Information for an atomic force microscopy (AFM) characterization of the electrodes fabricated with these shadow masks as well as with a commercially available shadow mask (Ossila E321, Ossila Ltd., Solpro Business Park, Windsor Street, Sheffield S4 7WB, UK).

3.2. Example of Devices Fabricated with the Shadow Masks

In order to illustrate the potential of these techniques to fabricate devices, we have deposited single-layer MoS₂ flakes bridging the electrodes fabricated by metal deposition through the shadow masks. We employed a viscoelastic dry-transfer method based on Gel-Film stamps [18] to transfer a single-layer MoS₂ flake to bridge the drain and source electrodes [19,20]. Figure 3a,c show optical microscopy images of devices fabricated with electrodes deposited through laser-ablated and vinyl + fiber shadow masks, respectively. After flake deposition, we perform a vacuum annealing step (2 h, 200 °C, 10⁻³ mbar) to improve the metal-semiconductor contact. We tested the electronic properties of the devices in a homebuilt probe station. Figure 3b,d show the source-drain current as a function of the back-gate voltage measured on the devices shown in Figure 3a,c. The transfer curves were measured under a constant source-drain bias V_{DS} of 1 V with a gate voltage step speed of 1 Vs⁻¹ (sweeping from -60 V to +60 V).

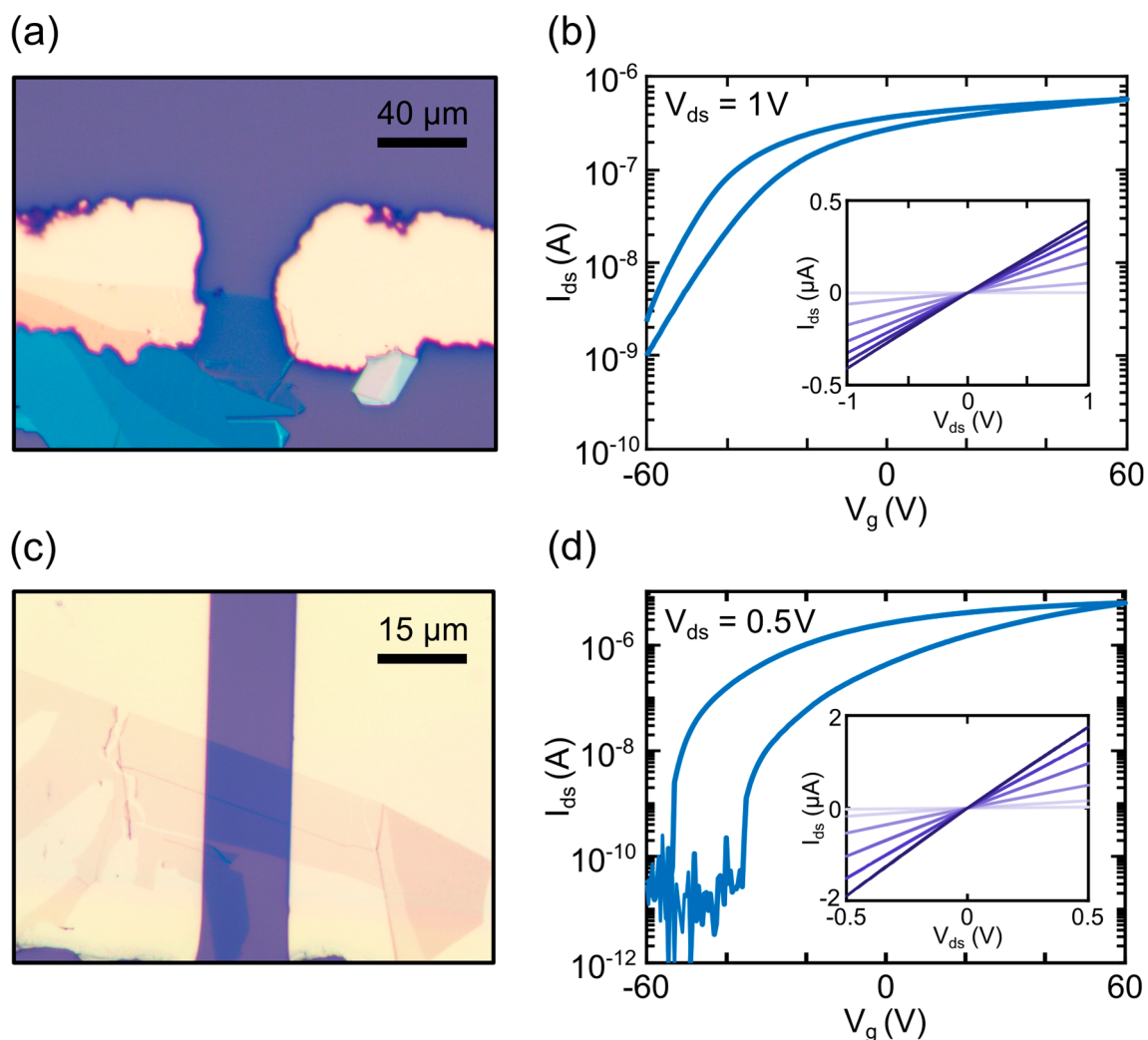


Figure 3. Example of nanomaterial-based devices based on the electrodes fabricated with the home-made shadow masks. (a) Optical microscopy image of a single-layer MoS₂ flake bridging the drain and source electrodes fabricated with the laser-ablated shadow mask. (b) Semi-logarithmic transfer curve of the resulting MoS₂ field-effect transistor for a constant bias V_{DS} of 1 V. (Inset) Gate-dependent IV s for gate voltages of -60 to 60 V. (c) Optical microscopy image of a transferred single-layer MoS₂ flake bridging the drain and source electrodes fabricated with vinyl + glass fiber mask. (d) Semi-logarithmic transfer curve of the resulting MoS₂ field-effect transistor for a constant bias V_{DS} of 0.5 V. (Inset) Gate-dependent IV s for gate voltages of -60 to 60 V.

From these measurements, one can extract the field-effect mobility (μ_{FE}) of the fabricated field-effect transistors by following this expression [21]:

$$\mu_{FE} = \frac{dI_{DS}}{dV_G} \frac{L}{W} \frac{1}{C_G \cdot V_{DS}} \quad (1)$$

where I_{DS} , V_{DS} , and V_{GS} are the source-drain current, source-drain voltage, and gate voltage, C_G is the capacitance of the silicon oxide dielectric, and L and W are the length and width of the transistor channel. The devices shown in Figure 3 presented a mobility of $0.94 \text{ cm}^2 \text{ V}^{-1} \text{ s}^{-1}$ (laser-ablation mask) and $10.7 \text{ cm}^2 \text{ V}^{-1} \text{ s}^{-1}$ (vinyl + fiber mask). In Figure S3 in the Supporting Information, the reader will find the results of another two devices showing mobilities of $1 \text{ cm}^2 \text{ V}^{-1} \text{ s}^{-1}$ (for the laser-ablation mask) and $0.39 \text{ cm}^2 \text{ V}^{-1} \text{ s}^{-1}$ (for the vinyl + fiber mask). These field-effect measurements have been carried out in a three-terminal configuration without discounting for the effect of the contact resistance, and thus, the mobility values obtained here should be considered lower-bound estimates, as discounting for the contact resistance would lead to larger mobilities. It is interesting to note that we found that devices fabricated with electrodes fabricated by deposition through commercially available shadow masks (Ossila E321) lead to devices with similar characteristics in terms of threshold voltage, mobility, and current ON/OFF values achieved by our group [22,23] as well as others [24–27], with typical mobility values below $10 \text{ cm}^2 \text{ V}^{-1} \text{ s}^{-1}$ when using SiO_2 as the dielectric material. Overcoming these values and getting closer to MoS_2 's theoretical limit of around $200 \text{ cm}^2 \text{ V}^{-1} \text{ s}^{-1}$ would mean a change to a dielectric material with a higher dielectric constant [21,22,28]. Similarly, other transistor architectures can be designed, such as simple complete bottom gate tunnel field-effect transistors [29,30] or anywhere where pre-patterned electrodes are applicable with consideration of the achievable feature sizes.

3.3. Examples of Shadow Masks with More Complex Patterns

Figure 4 shows a few examples of other shadow mask designs fabricated with the laser ablation method on $40 \mu\text{m}$ thick aluminum foil to illustrate the flexibility of this technique in the rapid prototyping of devices. These patterns are chosen due to their usefulness when studying nanomaterial-based devices: a Hall bar, a four-terminal mask, and a mask designed to test in-plane electrical anisotropy.

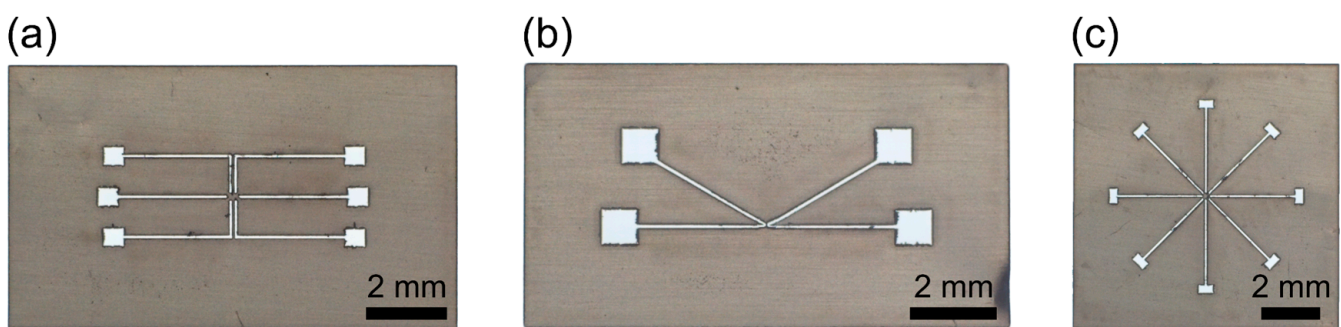


Figure 4. Examples of different shadow mask patterns created with the fiber laser engraving system. (a) Hall bar. (b) Four-terminal configuration. (c) Electrode probes to test in-plane anisotropic materials.

4. Discussion and Conclusions

We have presented two different approaches for fabricating shadow masks for the evaporation of electrodes onto nanomaterials using a commercially available fiber laser engraving system or a vinyl cutting machine. The laser engraving of aluminum foil is able to produce shadow masks with line widths of $50 \mu\text{m}$ and minimum feature separation of $20 \mu\text{m}$, although with a noticeable edge roughness and with complete flexibility over the pattern design. In the second technique, we use a vinyl cutter to define the pads and electrode leads, but we place a glass fiber to create a well-defined narrow separation

between the drain and source electrodes. This technique allows us to create line widths of 200 μm separated by 15 μm (dependent on the glass fiber diameter) with a very sharp and well-defined electrode separation. Nonetheless, the vinyl + fiber technique is less flexible than the laser engraving one in terms of prototyping. We have proven the potential of these techniques by fabricating devices based on MoS_2 . A set of different patterns shows the ability to extend this technique to various applications in the field of microelectronics without limitation of substrate type and the freedom of post-material assembly due to pre-patterned structures. By using this method, patterns on flexible substrates can enable measurements in the field of strain engineering or biomedical applications. Our approaches are cost-effective and easily accessible methods for fabricating shadow masks with high resolution and accuracy, making them accessible to a wider range of laboratories. This work contributes a valuable addition to the field of nanoelectronics by providing simple and inexpensive methods for fabricating high-resolution shadow masks.

Supplementary Materials: The following supporting information can be downloaded at <https://www.mdpi.com/article/10.3390/nanomanufacturing3030022/s1>. Figure S1: Mask fabrication on standard kitchen aluminum foil; Figure S2: Atomic force characterization of the electrodes fabricated with different techniques; Figure S3: More examples of nanomaterial-based devices based on the electrodes fabricated with the homemade shadow masks; Video S1: Shadow mask laser writing process.

Author Contributions: Conceptualization, A.C.-G. and T.P.; methodology, T.P. and P.B.; software, T.P.; validation, T.P. and A.C.-G.; formal analysis, T.P. and P.B.; data curation, T.P., P.B. and E.S.V.; writing—original draft preparation, A.C.-G.; writing—review and editing, A.C.-G. and T.P.; visualization, T.P., A.C.-G. and E.S.V.; supervision, A.C.-G. All authors have read and agreed to the published version of the manuscript.

Funding: This research was funded by the European Research Council (ERC) through the project grant agreement n^o 755655; the Ministry of Science and Innovation (Spain) through the projects PID2020-115566RB-I00 and TED2021-132267B-I00; the Horizon 2020 FLAG-ERA through the project To2Dox (JTC-2019-009); and Comunidad de Madrid through the project CAIRO-CM (Y2020/NMT-6661).

Data Availability Statement: The data of this study are available from the corresponding author upon reasonable request.

Acknowledgments: We thank Gulsum Ersu for her valuable help during the video shoot for the supporting information. This work was funded by the European Research Council (ERC) under the European Union's Horizon 2020 research and innovation program (grant agreement n^o 755655, ERC-StG 2017 project 2D-TOPSENSE) and the Ministry of Science and Innovation (Spain) through the projects PID2020-115566RB-I00 and TED2021-132267B-I00. We also acknowledge funding from the EU FLAG-ERA project To2Dox (JTC-2019-009) and the Comunidad de Madrid through the CAIRO-CM project (Y2020/NMT-6661). ChatGPT (GPT-3.5, OpenAI's large-scale language-generation model) was used to improve the English grammar and writing style of this manuscript. The authors have reviewed, edited, and revised the ChatGPT-generated texts to their own liking and take ultimate responsibility for the content of this publication [31].

Conflicts of Interest: The authors declare no conflict of interest.

References

1. Pugachev, M.V.; Duleba, A.I.; Galiullin, A.A.; Kuntsevich, A.Y. Micromask Lithography for Cheap and Fast 2D Materials Microstructures Fabrication. *Micromachines* **2021**, *12*, 850. [[CrossRef](#)] [[PubMed](#)]
2. Khan, M.S.; Lachmayer, R.; Roth, B. Maskless Lithography for Versatile and Low Cost Fabrication of Polymer Based Micro Optical Structures. *OSA Contin.* **2020**, *3*, 2808. [[CrossRef](#)]
3. Zhou, Y.X.; Johnson, A.T.; Hone, J.; Smith, W.F. Simple Fabrication of Molecular Circuits by Shadow Mask Evaporation. *Nano Lett.* **2003**, *3*, 1371–1374. [[CrossRef](#)]
4. Tien, D.H.; Park, J.-Y.; Kim, K.B.; Lee, N.; Seo, Y. Characterization of Graphene-Based FET Fabricated Using a Shadow Mask. *Sci. Rep.* **2016**, *6*, 25050. [[CrossRef](#)]

5. Bao, W.; Liu, G.; Zhao, Z.; Zhang, H.; Yan, D.; Deshpande, A.; LeRoy, B.; Lau, C.N. Lithography-Free Fabrication of High Quality Substrate-Supported and Freestanding Graphene Devices. *Nano Res.* **2010**, *3*, 98–102. [[CrossRef](#)]
6. Yun, H.; Kim, S.; Kim, H.; Lee, J.; McAllister, K.; Kim, J.; Pyo, S.; Sung Kim, J.; Campbell, E.E.B.; Hyoung Lee, W.; et al. Stencil Nano Lithography Based on a Nanoscale Polymer Shadow Mask: Towards Organic Nanoelectronics. *Sci. Rep.* **2015**, *5*, 10220. [[CrossRef](#)]
7. Liang, J.; Xu, K.; Toncini, B.; Bersch, B.; Jariwala, B.; Lin, Y.; Robinson, J.; Fullerton-Shirey, S.K. Impact of Post-Lithography Polymer Residue on the Electrical Characteristics of MoS₂ and WSe₂ Field Effect Transistors. *Adv. Mater. Interfaces* **2019**, *6*, 1801321. [[CrossRef](#)]
8. Shen, X.; Wang, H.; Yu, T. How Do the Electron Beam Writing and Metal Deposition Affect the Properties of Graphene during Device Fabrication? *Nanoscale* **2013**, *5*, 3352. [[CrossRef](#)]
9. Katagiri, Y.; Nakamura, T.; Ishii, A.; Ohata, C.; Hasegawa, M.; Katsumoto, S.; Cusati, T.; Fortunelli, A.; Iannaccone, G.; Fiori, G.; et al. Gate-Tunable Atomically Thin Lateral MoS₂ Schottky Junction Patterned by Electron Beam. *Nano Lett.* **2016**, *16*, 3788–3794. [[CrossRef](#)]
10. Cao, Y.; Mishchenko, A.; Yu, G.L.; Khestanova, E.; Rooney, A.P.; Prestat, E.; Kretinin, A.V.; Blake, P.; Shalom, M.B.; Woods, C.; et al. Quality Heterostructures from Two-Dimensional Crystals Unstable in Air by Their Assembly in Inert Atmosphere. *Nano Lett.* **2015**, *15*, 4914–4921. [[CrossRef](#)]
11. Castellanos-Gomez, A.; Vicarelli, L.; Prada, E.; Island, J.O.; Narasimha-Acharya, K.L.; Blanter, S.I.; Groenendijk, D.J.; Buscema, M.; Steele, G.A.; Alvarez, J.V.; et al. Isolation and Characterization of Few-Layer Black Phosphorus. *2D Mater.* **2014**, *1*, 025001. [[CrossRef](#)]
12. Aljada, M.; Mutkins, K.; Vamvounis, G.; Burn, P.; Meredith, P. High Quality Shadow Masks for Top Contact Organic Field Effect Transistors Using Deep Reactive Ion Etching. *J. Micromech. Microeng.* **2010**, *20*, 075037. [[CrossRef](#)]
13. Zhang, H.; Guo, X.; Niu, W.; Xu, H.; Wu, Q.; Liao, F.; Chen, J.; Tang, H.; Liu, H.; Xu, Z.; et al. Multilayer Si Shadow Mask Processing of Wafer-Scale MoS₂ Devices. *2D Mater.* **2020**, *7*, 025019. [[CrossRef](#)]
14. Tomczyk, M.; Kubik, P.; Waliszewski, W. Optimization of the Ablative Laser Cutting of Shadow Mask for Organic FET Electrode Fabrication. *Electronics* **2020**, *9*, 2184. [[CrossRef](#)]
15. Elhami Nik, F.; Matthiesen, I.; Herland, A.; Winkler, T. Low-Cost PVD Shadow Masks with Submillimeter Resolution from Laser-Cut Paper. *Micromachines* **2020**, *11*, 676. [[CrossRef](#)] [[PubMed](#)]
16. Staley, N.; Wang, H.; Puls, C.; Forster, J.; Jackson, T.N.; McCarthy, K.; Clouser, B.; Liu, Y. Lithography-Free Fabrication of Graphene Devices. *Appl. Phys. Lett.* **2007**, *90*, 143518. [[CrossRef](#)]
17. Castellanos-Gomez, A.; Smit, R.H.M.; Agrait, N.; Rubio-Bollinger, G. Spatially Resolved Electronic Inhomogeneities of Graphene Due to Subsurface Charges. *Carbon* **2012**, *50*, 932–938. [[CrossRef](#)]
18. Castellanos-Gomez, A.; Buscema, M.; Molenaar, R.; Singh, V.; Janssen, L.; van der Zant, H.S.J.; Steele, G.A. Deterministic Transfer of Two-Dimensional Materials by All-Dry Viscoelastic Stamping. *2d Mater.* **2014**, *1*, 011002. [[CrossRef](#)]
19. Yang, R.; Zheng, X.; Wang, Z.; Miller, C.J.; Feng, P.X.-L. Multilayer MoS₂ Transistors Enabled by a Facile Dry-Transfer Technique and Thermal Annealing. *J. Vac. Sci. Technol. B Nanotechnol. Microelectron. Mater. Process. Meas. Phenom.* **2014**, *32*, 61203.
20. Frisenda, R.; Navarro-Moratalla, E.; Gant, P.; De Lara, D.P.; Jarillo-Herrero, P.; Gorbachev, R.V.; Castellanos-Gomez, A. Recent Progress in the Assembly of Nanodevices and van Der Waals Heterostructures by Deterministic Placement of 2D Materials. *Chem. Soc. Rev.* **2018**, *47*, 53–68. [[CrossRef](#)]
21. Radisavljevic, B.; Radenovic, A.; Brivio, J.; Giacometti, V.; Kis, A. Single-Layer MoS₂ Transistors. *Nat. Nanotechnol.* **2011**, *6*, 147–150. [[CrossRef](#)]
22. Puebla, S.; Pucher, T.; Rouco, V.; Sanchez-Santolino, G.; Xie, Y.; Zamora, V.; Cuellar, F.A.; Mompean, F.J.; Leon, C.; Island, J.O.; et al. Combining Freestanding Ferroelectric Perovskite Oxides with Two-Dimensional Semiconductors for High Performance Transistors. *Nano Lett.* **2022**, *22*, 7457–7466. [[CrossRef](#)] [[PubMed](#)]
23. Xie, Y.; Çakıroğlu, O.; Hu, W.; He, K.; Puebla, S.; Pucher, T.; Zhao, Q.; Ma, X.; Munuera, C.; Castellanos-Gomez, A. Laser Trimming for Lithography-Free Fabrications of MoS₂ Devices. *Nano Res.* **2023**, *16*, 5042–5046. [[CrossRef](#)]
24. Qiu, H.; Pan, L.; Yao, Z.; Li, J.; Shi, Y.; Wang, X. Electrical Characterization of Back-Gated Bi-Layer MoS₂ Field-Effect Transistors and the Effect of Ambient on Their Performances. *Appl. Phys. Lett.* **2012**, *100*, 123104. [[CrossRef](#)]
25. Late, D.J.; Liu, B.; Matte, H.S.S.R.; Dravid, V.P.; Rao, C.N.R. Hysteresis in Single-Layer MoS₂ Field Effect Transistors. *ACS Nano* **2012**, *6*, 5635–5641. [[CrossRef](#)] [[PubMed](#)]
26. Ghatak, S.; Pal, A.N.; Ghosh, A. Nature of Electronic States in Atomically Thin MoS₂ Field-Effect Transistors. *ACS Nano* **2011**, *5*, 7707–7712. [[CrossRef](#)]
27. Li, T.; Du, G.; Zhang, B.; Zeng, Z. Scaling Behavior of Hysteresis in Multilayer MoS₂ Field Effect Transistors. *Appl. Phys. Lett.* **2014**, *105*, 093107. [[CrossRef](#)]
28. Yoon, Y.; Ganapathi, K.; Salahuddin, S. How Good Can Monolayer MoS₂ Transistors Be? *Nano Lett.* **2011**, *11*, 3768–3773. [[CrossRef](#)]
29. Nourbakhsh, A.; Zubair, A.; Dresselhaus, M.S.; Palacios, T. Transport Properties of a MoS₂/WSe₂ Heterojunction Transistor and Its Potential for Application. *Nano Lett.* **2016**, *16*, 1359–1366. [[CrossRef](#)]

30. Balaji, Y.; Smets, Q.; Szabo, Á.; Mascaro, M.; Lin, D.; Asselberghs, I.; Radu, I.; Luisier, M.; Groeseneken, G. MoS₂/MoTe₂ Heterostructure Tunnel FETs Using Gated Schottky Contacts. *Adv. Funct. Mater.* **2020**, *30*, 1905970. [[CrossRef](#)]
31. Castellanos-Gomez, A. Good Practices for Scientific Article Writing with ChatGPT and Other Artificial Intelligence Language Models. *Nanomanufacturing* **2023**, *3*, 135–138. [[CrossRef](#)]

Disclaimer/Publisher's Note: The statements, opinions and data contained in all publications are solely those of the individual author(s) and contributor(s) and not of MDPI and/or the editor(s). MDPI and/or the editor(s) disclaim responsibility for any injury to people or property resulting from any ideas, methods, instructions or products referred to in the content.